analytical chemistry

Article

pubs.acs.org/ac

Label-Free Raman Spectroscopic Imaging Monitors the Integral Physiologically Relevant Drug Responses in Cancer Cells

Samir F. El-Mashtoly,[†,§] Hesham K. Yosef,[†,§] Dennis Petersen,[†] Laven Mavarani,[†] Abdelouahid Maghnouj,[‡] Stephan Hahn,[‡] Carsten Kötting,[†] and Klaus Gerwert*[,†]

[†]Department of Biophysics and [‡]Department of Molecular GI-Oncology, Clinical Research Center, Ruhr-University Bochum, 44780 Bochum, Germany

Supporting Information

ABSTRACT: Predictions about the cellular efficacy of drugs tested *in vitro* are usually based on the measured responses of a few proteins or signal transduction pathways. However, cellular proteins are highly coupled in networks, and observations of single proteins may not adequately reflect the *in vivo* cellular response to drugs. This might explain some large discrepancies between *in vitro* drug studies and drug responses observed in patients. We present a novel *in vitro* marker-free approach that enables detection of cellular responses to a drug. We use Raman spectral imaging to measure the effect of the epidermal growth factor receptor (EGFR) inhibitor panitumumab on cell lines expressing wild-type Kirsten-Ras (K-Ras) and oncogenic K-Ras mutations. Oncogenic K-Ras mutation blocks the response to anti-EGFR therapy in patients, but this effect is not readily observed *in vitro*. The Raman studies detect large panitumumab-induced differences *in vitro* in cells harboring wild-type K-Ras as seen in A in red but not in cells with K-Ras mutations as seen in B; these studies reflect the observed patient outcomes. However, the effect is not observed when extracellular-signal-regulated kinase phosphorylation is monitored. The Raman spectra show for cells with wild-type K-Ras alterations based on the responses to panitumumab. The subcellular component with the largest spectral response to panitumumab was lipid droplets, but this effect was not observed when cells harbored K-Ras mutations. This study develops a noninvasive, label-free, *in vitro* vibrational spectroscopic test to determine the integral physiologically relevant drug response in cell lines. This approach opens a new field of patient-centered drug testing that could deliver superior patient therapies.

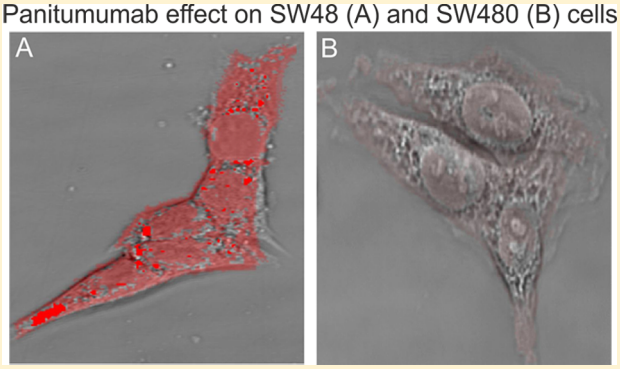

There is a tremendous need for the development of a practical, noninvasive, and high throughput analytical method to evaluate the potency and efficacy of drug candidates *in vitro* during early stages of drug discovery. Current methods include Western blotting and fluorescence spectroscopy of labeled marker proteins, which monitor individual proteins and single signal transduction pathways. However, systems biology shows that proteins are highly coupled within networks. Cross-talk, feedback loops, and compensation by other pathways can affect cellular drug responses and in some cases can completely block drug efficacy.[1]

A complete understanding of complex protein networks and cellular signaling pathways is the ultimate goal. However, a simple *in vitro* test is needed to indicate the overall physiological response of a given cell line to a specific drug, which is in agreement with the clinically observed patient response. This test would be a powerful complementary tool to evaluate drug efficacy, even when a deep understanding of individual signaling pathways is lacking. Current methods utilize fluorescence spectroscopy to monitor single proteins marked by antibodies or fluorescent dyes. By contrast, Raman spectroscopy provides a spectral read-out of the integral biochemical status of multiple cellular components. The difference spectra of the cellular status before and after drug application detect the integral biochemical response to the drug (see below). Here, we explore this approach by Raman spectroscopy of the cellular response to the commonly used antiepidermal growth factor receptor (EGFR) cancer drug panitumumab.

Manipulating the EGFR pathway is one of the primary strategies for targeted cancer therapy.[2−4] EGFR is overexpressed in numerous tumors of the breast, head, neck, lung, bladder, colon, cervix, kidneys, and brain. EGFR overexpression promotes tumorigenesis by modulating cell proliferation, angiogenesis, and metastasis.[5−9] EGFR is a transmembrane tyrosine kinase receptor that contains an extracellular ligand-binding domain, a transmembrane domain, and an intracellular tyrosine kinase domain. Binding of ligands such as epidermal

Received: April 16, 2015
Accepted: June 15, 2015
Published: June 15, 2015

DOI: 10.1021/acs.analchem.5b01431
Anal. Chem. 2015, 87, 7297−7304

growth factor (EGF) to EGFR induces receptor dimerization and autophosphorylation of the tyrosine kinase domain. Panitumumab (Vectibix) is the first fully human monoclonal antibody specific for EGFR to enter clinical trials for the treatment of solid tumors. It was approved by the U.S. Food and Drug Administration for the treatment of patients with EGFR-overexpressing metastatic colorectal cancer. Panitumumab blocks EGF binding to the EGFR ligand-binding site, induces internalization of the receptor-antibody complex, and down-regulates EGFR activity. This blocks ligand-induced EGFR tyrosine autophosphorylation and subsequent activation of signaling pathways involved in carcinogenesis. Panitumumab especially blocks activation of the MAP kinase pathway, which modulates cellular proliferation and survival, as shown in Figure 1,[5,6] and promotes apoptosis and inhibits cell proliferation and angiogenesis.

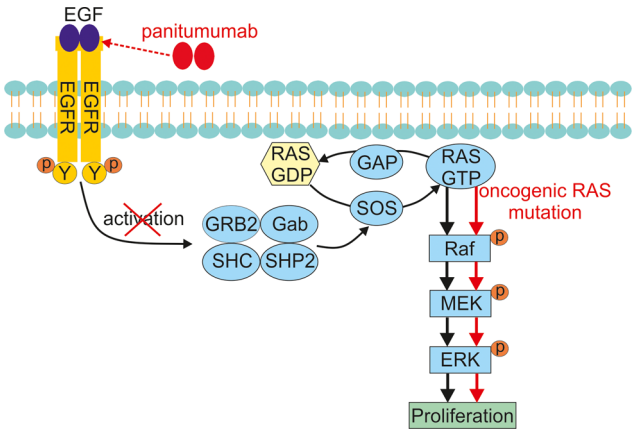

Figure 1. Ras signal transduction pathway.[13]

Ras proteins are small GTPases that act as molecular switches with on and off states. GDP is bound to Ras in the off state, whereas GTP is bound to Ras in the on state.[10,11] Ras regulates cellular responses to several extracellular stimuli, including EGF. EGF binding to the EGFR receptor at the cell surface activates receptor complexes that contain several adaptor proteins (Figure 1). Ras-GTP interacts with several effector proteins and stimulates their catalytic activity to regulate cellular responses such as survival, proliferation, and differentiation.[12,13] Mutations in one of the RAS genes converts them into active oncogenes.[14] Ras gene mutations have been identified in pancreatic, colon, lung, and thyroid tumors and in myeloid leukemia, although the incidence differs among different cancers.[14] For example, Kirsten-Ras (K-Ras) oncogenic mutations result in constitutive activation, and have been identified in approximately 30−50% of patients with advanced colorectal carcinoma.[5]

Ras is located downstream of EGFR. Oncogenic Ras mutation results in uncontrolled activation of the MAP kinase pathway that is independent of EGFR (Figure 1). Therefore, targeting EGFR is an ineffective therapeutic strategy. Several clinical studies have shown that oncogenic K-Ras mutations block the efficacy of panitumumab therapy.[15−17] Patients with colorectal carcinoma must be screened for K-Ras mutations before using cost-intensive panitumumab treatment. However, to the best of our knowledge, there is no experimental evidence showing the *in vitro* impact of K-Ras mutations on panitumumab efficacy in cells.

Raman vibrational spectroscopic imaging has emerged as a powerful tool for the analysis of biological samples. It is noninvasive and cost-effective and does not require extrinsic labels or dyes. Raman spectral imaging has been used for classification of human cancer tissues[18,19] and to image cellular organelles.[20−26] Raman spectroscopy can be used to resolve and track cellular uptake of liposomal drug-carrier systems[27−29] and the cellular distribution of chemotherapeutics and molecular drugs.[30−35] Raman imaging has been used to investigate the interaction of several chemotherapeutic agents in a variety of cancer cells.[36−41] A recent study used Raman spectroscopy to investigate the effect of *cis*-platin on lung cancer cells.[40,41] However, to our knowledge, the integral physiologically relevant response of individual cellular components to drugs has not been investigated by Raman spectral imaging. Here, we used Raman imaging to detect cellular responses to the EGFR inhibitor panitumumab. Raman hyperspectral images of colon cancer cells were analyzed with multivariate methods such as hierarchical cluster analysis (HCA). We identified subcellular organelles by comparing the HCA pseudocolor images with those obtained by fluorescence microscopy. We report the first *in vitro*, label-free spectroscopic evidence that detects the effect of oncogenic K-Ras mutations on the cellular response to panitumumab by using colon cancer SW48 and SW480 cells that are harboring wild-type K-Ras and oncogenic K-Ras mutations, respectively. The *in vitro* results are in agreement with the clinically observed patient responses. The results indicate that colon cancer cells harboring the wild-type K-Ras experience a strong and physiologically relevant response to panitumumab treatment, whereas colon cancer cells expressing oncogenic K-Ras mutations do not experience physiologically relevant responses to panitumumab. The largest response occurred in lipid droplets of cancer cells harboring wild-type K-Ras that were treated with panitumumab.

EXPERIMENTAL SECTION

Cell Culture. Human colorectal adenocarcinoma SW48 (CCL-231) and SW480 (CCL-228) cells were obtained from the American Type Culture Collection. Cells were cultured in Dulbecco's modified Eagle's medium (DMEM; Invitrogen, Carlsbad, USA) supplemented with 10% fetal bovine serum (FBS; Invitrogen, Carlsbad, USA), 2 mM L-glutamine, and 5% penicillin/streptomycin and incubated at 37 °C in a 10% CO_2 atmosphere. Raman measurements were performed on cells grown on CaF_2 windows (Korth Kristalle, Kiel, Germany) to avoid background signals from conventional glass slides. Cells were incubated with either EGF (100 ng/mL) or panitumumab (10 μg/mL) at 37 °C in a 10% CO_2 atmosphere for 15 min and 12 h, respectively. Then, cells were fixed in 4% paraformaldehyde (VWR International, Darmstadt, Germany) and submerged in phosphate-buffered saline (PBS; Invitrogen, Carlsbad, USA).

Confocal Raman Microscopy. Raman spectroscopic imaging was performed using a WITec alpha 300AR confocal Raman microscope (Ulm, Germany) as described previously.[18,35] A frequency-doubled Nd:YAG laser of 532 nm (Crystal Laser, Reno, USA) was used as an excitation source with an output power of approximately 40 mW. The laser radiation was coupled into a Zeiss microscope through a wavelength-specific single-mode optical fiber. The laser beam was collimated via an achromatic lens and passed through a holographic band-pass filter before being focused on the sample

DOI: 10.1021/acs.analchem.5b01431
Anal. Chem. 2015, 87, 7297−7304

through a Nikon NIR APO (60×/1.00 NA) water-immersion objective. The laser excitation spot size is ∼1 μm. The sample was located on a piezoelectrically driven microscope scanning stage of an *x,y* resolution of ∼3 ± 5 nm and *z* resolution of ∼0.3 ± 2 nm. Raman backscattered light was collected through a microscopic objective and passed through a holographic edge filter onto a multimode fiber (50 μm diameter) and into a 300 mm focal length monochromator, which incorporated a 600/mm grating blazed at 500 nm. Raman spectra were detected by a back-illuminated deep-depletion charge coupled device (CCD) camera operating at −60 °C. Raman imaging measurements are acquired by raster-scanning the laser beam over cells and collecting a full Raman spectrum at speed of 0.5 s per pixel and the pixel resolution is 500 nm.

Multivariate Analysis. The Raman spectra of cells were analyzed using HCA. Raman hyperspectral results were imported into MATLAB 8.2 (MathWorks Inc., MA), and data preprocessing and multivariate analyses were performed using in-house built scripts. Raman spectra that had no C−H band at 2850−3000 cm^{-1} were treated as background and deleted. Cosmic spikes were removed using an impulse noise filter, and Raman spectra were interpolated to a reference wavenumber scale. All spectra were then baseline-corrected using a third-order polynomial and were vector normalized. We performed HCA on the regions of 700−1800 and 2800−3050 cm^{-1} using Ward's clustering in combination with the Pearson correlation distance. The Raman difference spectra were calculated using normalized average spectra with the Phe band near 1008 cm^{-1}.

RESULTS AND DISCUSSION

EGF Binding to EGFR. To monitor the effect of EGF binding to EGFR, several Raman measurements of SW48 and SW480 cells (approximately 50 cells per cell line) were performed. SW48 cells harbor wild-type K-Ras, whereas SW480 cells express oncogenic K-Ras mutations. The Raman difference spectra of control cells versus cells treated with EGF are presented in Figure 2. The spectra reflect the overall cell responses to EGF. Large spectral changes were observed for SW48 cells (Figure 2). This result demonstrates that EGF activation of EGFR is reflected by changes in the Raman difference spectrum. However, SW480 cells expressing oncogenic K-Ras mutations have constitutive MAP kinase activation, and EGF activation of the EGFR receptor no longer influences the MAP kinase pathway. The Raman difference spectra for SW480 cells showed no significant cellular response to EGF (Figure 2). These spectra confirm that Raman microscopy detects physiologically relevant cellular responses.

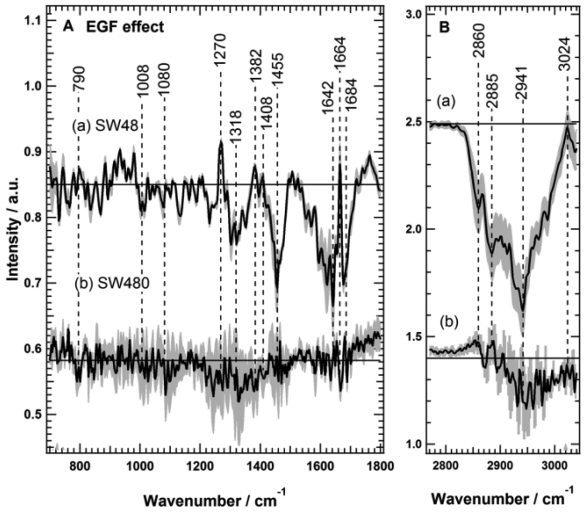

Figure 2. Effect of EGF on SW48 (a) and SW480 (b) cells. Raman difference spectra of control cells versus EGF-treated cells in the 700−1800 (A) and 2770−3040 cm^{-1} (B) regions reflect the changes occurring in cells. Shading represents the standard deviation. The spectra have been offset for clarity.

Next, we improved the spatial resolution of the response. The feasibility of using Raman spectral imaging coupled with HCA to visualize subcellular organelles was demonstrated recently.[42−44]

In the present study, subcellular components were identified by Raman spectroscopy combined with HCA in addition to fluorescence microscopy, which was used as a reference. Figure 3A shows a bright-field image of SW48 cells in PBS buffer.

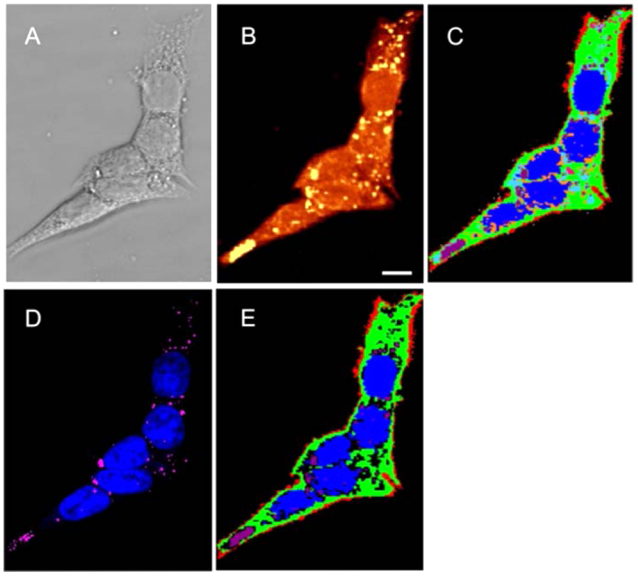

Figure 3. Comparison of Raman and fluorescence microscopic imaging. (A) Bright-field image of SW48 cells. (B) Integrated Raman intensities in the C−H stretching region of SW48 cells shown in A. (C) HCA results based on the Raman data shown in B. (D) Fluorescence imaging of nuclei (blue) and lipid droplets (magenta). (E) HCA clusters of membrane (red), cytoplasm (green), nuclei (blue), and lipid droplets (magenta). Scale bar = 10 μm.

SW48 cells have a characteristic shape and are typically 15−20 μm in diameter. Figure 3B shows a univariate image based on the integrated Raman intensities of the C−H stretching vibration in the 2800−3100 cm^{-1} region. This image most likely shows nuclei and lipid droplets in the cytoplasm. Figure 3C shows the HCA image, which is generated from Raman hyperspectral data. The HCA algorithm searches for similar spectra and groups them into so-called clusters. The merging process is repeated until all Raman spectra are combined into a small number of clusters and each cluster has a defined color, which results in an index-colored image. HCA was performed on the spectral ranges of 700−1800 and 2800−3100 cm^{-1}. These spectral regions exhibit the major vibrational bands that originate from amino acids, protein backbones, nucleotides, nucleic acid backbones, carbohydrates, and lipids. These

DOI: 10.1021/acs.analchem.5b01431
Anal. Chem. 2015, 87, 7297−7304

vibrational bands contain sufficient spectral information to give excellent clustering results. Ten clusters were selected to reproduce the position of nuclei (blue) and lipid droplets (magenta, the lowest size of lipid droplets is around 0.7−0.8 μm), in addition to various subcellular components in the cytoplasm.

To identify nuclei and lipid droplets, cells were stained with DRAQ-5 and Nile Red, respectively, and fluorescence microscopy was performed on the same sample (Figure 3D) that had been used for Raman spectral imaging. The results show that the nucleus is the largest cellular component in SW48 cells, and lipid droplets are distributed in the cytoplasm surrounding the nucleus. By comparing the fluorescence image (Figure 3D) with the HCA index-color image (Figure 3C), it is reasonable to assign the blue and magenta clusters in the HCA image to nuclei and lipid droplets, respectively. Lipid droplets also are identified by their Raman spectra, which are characterized by the strong intensity of approximately all Raman bands (see below).[45−49] The morphology and topology of some clusters in Figure 3C clearly suggest that they are associated with the plasma membrane (red) and cytoplasm (green). For example, the outermost cluster in Figure 3C is assigned to the plasma membrane. This also is based on fluorescence imaging of EGFR, which is located in the plasma membrane (Figure S1 in Supporting Information (SI)). Figure 3E shows only the identified cellular components, including the plasma membrane, cytoplasm, nuclei, and lipid droplets.

The average cluster spectra of subcellular organelles are presented in Figure 4. The Raman spectra contain C−H

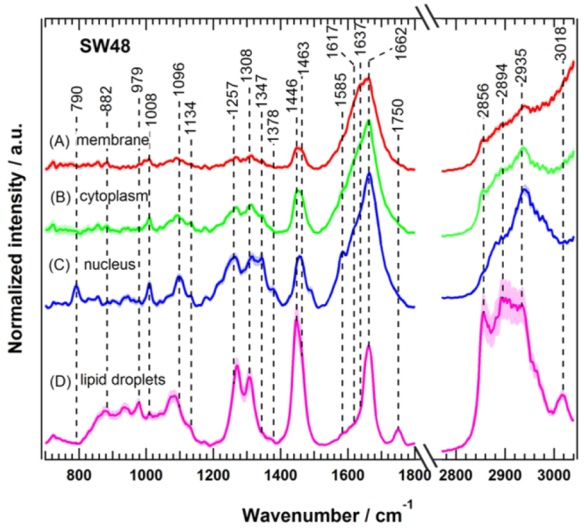

Figure 4. Average cluster Raman spectra of plasma membrane (A), cytoplasm (B), nucleus (C), and lipid droplets (D) in the 700−1800 and 2770−3040 cm^{-1} regions. Shading represents the standard deviation. The spectra have been offset for clarity.

stretching modes (CH_3, CH_2, and CH) located near 2800−3020 cm^{-1}, carbonyl stretching modes (amide I) located at 1662 cm^{-1}, and C−H and CH_2 bending deformation modes located at 1446 cm^{-1}. The amide III mode of peptide linkages is located near 1230 and 1380 cm^{-1}, and the phenylalanine ring-breathing mode is located at 1008 cm^{-1}.[42,50,51] There is a similarity between the Raman spectra of the membrane (Figure 4A) and cytoplasm (Figure 4B). This is because the laser excitation spot size is <1 μm and the plasma membrane is much smaller than this value, suggesting that the cytoplasm (and perhaps the buffer) partially contributes to the membrane spectrum. However, the intensity ratio of 1446/1662 cm^{-1} bands is different in the membrane (Figure 4A) and cytoplasm (Figure 4B) spectra. The membrane spectrum has an additional shoulder at ∼1637 cm^{-1}. Only the nucleus spectrum (Figure 4C) contains a Raman band at 790 cm^{-1}, which is a DNA marker (O−P−O backbone stretching). By contrast, the spectrum in Figure 4D significantly differs from the others and exhibits strong-intensity bands throughout the whole spectrum (these are not seen in Figure 4 due to spectral normalization).

Only the spectrum in Figure 4D contains Raman bands at 1750 and 3018 cm^{-1}, which are attributed to the C═O stretching vibration of fatty acid ester forms and the ═C——H stretching mode of unsaturated fatty acids, respectively. By comparing the spectrum in Figure 4D with those of lipids and phospholipids,[45−49] it is clear that the spectrum in Figure 4D originates from high lipid or phospholipid content. In summary, these experiments show that membranes, cytoplasm, nuclei, and lipid droplets have characteristic Raman spectra that may be useful for examining the effects of ligand- or drug-binding to EGFR.

Nawaz et al.[41] performed Raman measurements across selected points in the specified subcellular regions of lung cancer cells to investigate the effect of range of *cis*-platin doses on the plasma membrane, cytoplasm, and nucleus. The selection of Raman spectra for each cellular component was based only on visual inspection, without clear identification of the cellular components.[41] By contrast, we clearly identified the Raman spectral images of three components such as nuclei, lipid droplets (Figure 3), and plasma membrane (Figure S1 in SI), by comparison with fluorescence microscopic images and characteristic Raman spectral bands.

Figure 5A presents the difference spectra of plasma membrane, cytoplasm, nucleus, and lipid droplets in SW48 cells with wild-type K-Ras exposed to EGF. The membrane difference spectrum (a) yields negative features at 1250−1350 cm^{-1} (amide III), 1453 cm^{-1} (C−H deformation), 1674 cm^{-1} (amide I), and 2850−2950 cm^{-1} (C−H stretching), indicating that the intensity of these bands increases in EGF-treated cells compared with control cells. The changes in amide I and III are associated with proteins, whereas the change in C−H stretching and deformation originates from membrane lipids. The cytoplasm difference spectrum (b) also displays negative peaks that are similar to those observed for the membrane (a); however, the cytoplasm spectral changes are larger than those of the membrane. Only the nucleus difference spectrum (c) exhibits a positive peak at 790 cm^{-1}, which is associated with O−P−O backbone stretching of DNA. The nucleus difference spectrum also displays negative peaks at 1453 and 2850−2950 cm^{-1}. The largest spectral changes observed in cells in response to EGF are detected in the difference spectrum of lipid droplets (d). For example, strong positive peaks are observed at approximately 939, 979, 1082, 1272, 1453, and 3021 cm^{-1}. The bandwidth of the Raman band centered at 1662 cm^{-1} is significantly increased in the lipid droplet difference spectrum, along with a slight wavenumber down-shift by ∼2 cm^{-1} on EGF binding; as a result, two negative peaks appear in the difference spectrum (d) at 1627 and 1689 cm^{-1}. EGF is reported to regulate the secretion and formation of lipids in cells, and triglyceride secretion in Caco-2 colon cancer cells is stimulated by EGF.[52] EGF also increases the

DOI: 10.1021/acs.analchem.5b01431
Anal. Chem. 2015, 87, 7297−7304

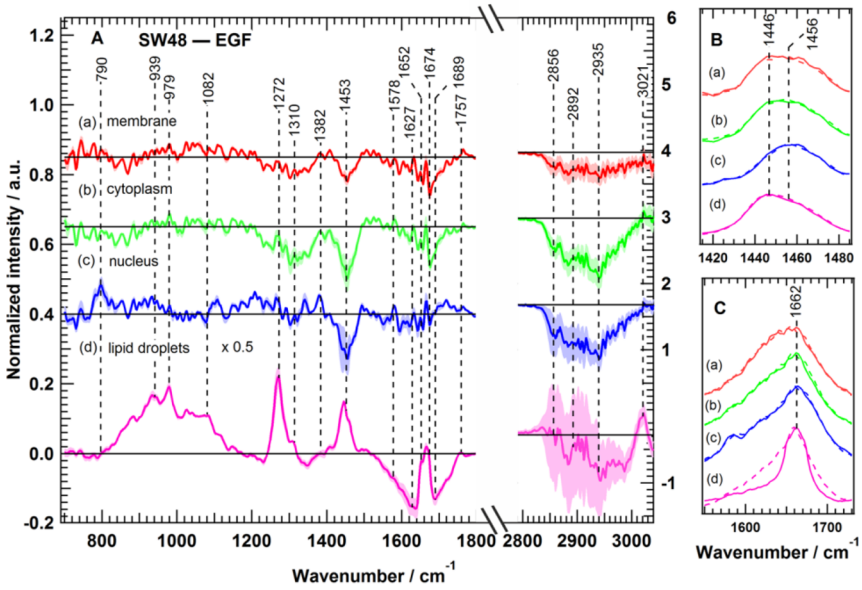

Figure 5. Effect of EGF ligand on SW48 subcellular components. (A) Raman difference spectra of control cells versus cells exposed to 10 ng/mL EGF for plasma membrane (a), cytoplasm (b), nucleus (c), and lipid droplets (d). Shading represents the standard deviation. Average Raman spectra of control cells (solid lines) and cells incubated with EGF (broken lines) in the (B) 1415−1485 cm^{-1} and (C) 1550−1730 cm^{-1} regions. Average spectra are normalized with the 1450 and 1660 cm^{-1} bands in B and C, respectively. The spectra have been offset for clarity.

intracellular cholesterol and triglyceride levels in C2BBel colon cancer cells.[53] Therefore, we suggest that broadening of the Raman band at 1662 cm^{-1} occurs as a result of EGF-induced increases in triglyceride and cholesterol levels in cells. These results show for the first time that noninvasive Raman spectroscopy efficiently detects the effects of EGF−EGFR binding on subcellular components.

To confirm that receptor internalization occurs in cells under our experimental conditions, cells were labeled with EGFR-specific antibodies, and fluorescence microscopy (Figure S2, SI) was performed after Raman spectral imaging. As expected, most of the EGFR was associated with the plasma membrane in the absence of EGF, whereas EGFR was internalized in the presence of EGF in both SW48 and SW480 cells. Western blotting analyses were performed with phosphospecific antiextracellular-signal-regulated kinase (ERK) 1 and anti-ERK2 antibodies to assess ERK1/2 phosphorylation (Figure 6). SW48 cells displayed some ERK phosphorylation in the absence of EGF (Figure 6A), but it increased significantly in the presence of EGF. This result indicates that the MAP kinase pathway is activated by EGFR activation. SW48 cells carry a mutant EGFR allele that probably contributed to basal ERK activation.[54] The fluorescence and Western blotting results are in agreement with those reported previously[54−56] and indicate that the observed changes in the Raman difference spectra of subcellular components (Figure 5) are produced as a result of EGFR activation. The MAP kinase pathway is not activated in the presence of panitumumab independent of the presence of EGF. Similar results were observed in SW480 cells that carry oncogenic K-Ras mutations. One would expect that the MAP kinase pathway is constitutively activated (Figure 1) and that EGF and panitumumab do not produce effective cellular responses, as observed in patients with oncogenic K-Ras mutations that do not respond to panitumumab treatment. Therefore, we tested whether our Raman spectroscopic assay was consistent with observed patient responses.

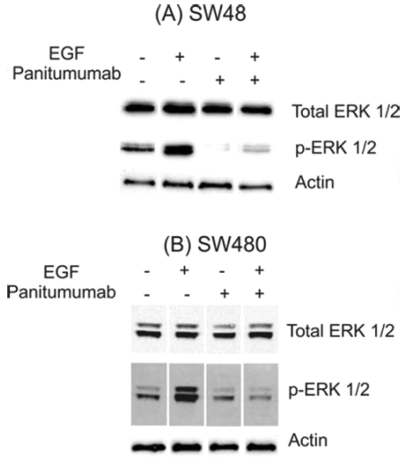

Figure 6. Effect of EGF and panitumumab on ERK activation in (A) SW48 and (B) SW480 colon cancer cells. Cell lysates were resolved by SDS-PAGE and Western blot analysis using antibodies that recognize phosphospecific ERK1 and ERK2 (p-ERK1/2) or total ERK1 and ERK2 (ERK1/2). β-actin was used as a loading control.

Panitumumab Binding to EGFR. Panitumumab binds with high affinity to an EGFR extracellular domain, competitively blocks EGF binding to the receptor, and causes internalization of the receptor−antibody complex. This prevents ligand-induced activation and arrests tumor cell proliferation.[57,58]

To detect the effect of panitumumab binding to EGFR on cells, we performed Raman measurements of control cells (SW48 and SW480) and cells exposed to 10 μg/mL of panitumumab. This concentration is equivalent to the manufacturer's recommended dose for clinical application of panitumumab (6 mg/kg). Essentially all cells are viable at this concentration, as indicated by the cytotoxicity assay (Figure S3, SI). The Raman difference spectra of control cells versus panitumumab-treated cells are shown in Figure S4 (SI).

DOI: 10.1021/acs.analchem.5b01431
Anal. Chem. 2015, 87, 7297−7304

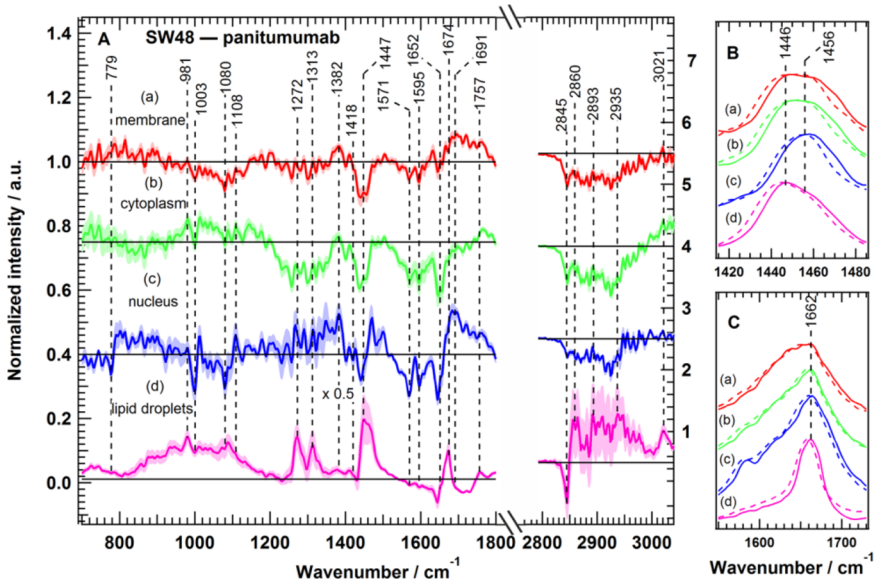

Figure 7. Effect of panitumumab on SW48 subcellular components. (A) Raman difference spectra of control cells versus cells exposed to 10 μg/mL panitumumab for plasma membrane (a), cytoplasm (b), nucleus (c), and lipid droplets (d). Shading represents the standard deviation. Average spectra are normalized with the 1450 and 1660 cm^{-1} bands in B and C, respectively. The spectra have been offset for clarity.

Panitumumab was not detected in these spectra because its concentration is below the detection limit. Large spectral changes were detected for SW48 cells, whereas no significant spectral changes were observed for SW480 cells. These results suggest that oncogenic K-Ras mutations have a crucial role in determining the efficacy of panitumumab chemotherapy.

To identify the cellular components in SW48 cells that display panitumumab-induced spectral changes, we performed HCA and identified cellular components similar to the methods used for the data in Figures 3 and 4. Figure 7A shows the difference spectra for the plasma membrane (a), cytoplasm (b), nucleus (c), and lipid droplets (d) of control cells versus panitumumab-treated cells. The membrane difference spectrum (a) reveals spectral changes, some of which are due to proteins and detected at 1652 cm^{-1} (amide I). Negative bands are detected at 1080 cm^{-1} (phosphodiester group), 1446 cm^{-1} (C−H deformation), and 2850−2950 cm^{-1} (C−H stretching), which are associated with membrane lipids. Panitumumab-induced wavenumber shifts are observed for the C−H deformation band near 1456−1453 cm^{-1} (Figure 7B) and for the amide I band near 1662−1658 cm^{-1} (Figure 7C). Larger spectral changes associated with proteins and lipids are observed in the cytoplasm difference spectrum (Figure 7A). For example, the changes at ∼1003 cm^{-1} (phenylalanine ring-breathing mode), 1250−1350 cm^{-1} (amide III), and 1652 cm^{-1} (amide I) arise from proteins, whereas strong negative bands at 1447 and 2850−2950 cm^{-1} originate from lipids. Although the 1447 cm^{-1} band had a wavenumber shift (Figure 7B) after panitumumab treatment, it is observed as a negative peak in the difference spectrum (Figure 7A) instead of a derivative-like shape. This is because the wavenumber shift is coupled with significant intensity change, which results in a negative peak.

Several spectral changes are observed in the nucleus difference spectrum (Figure 7A). For example, negative peaks occur at 779, 1003, 1447, 1571, 1595, 1652, and 2850−2950 cm^{-1}. The nucleus difference spectrum also has derivative-like peaks at 1652/1674 cm^{-1}, which are produced from wavenumber downshift of the amide I vibration (obvious in Figure 7C). Significant strong spectral changes are observed in the lipid droplet difference spectrum (Figure 7A) at 981, 1080, 1272, 1313, 1447, 1757, 2845, and 2860 cm^{-1}. A derivative-like shape also appears at 1645/1674 cm^{-1}, implying that amide I has a panitumumab-induced wavenumber shift (clearly seen in Figure 7C). Thus, panitumumab treatment exerts strong effects on lipid droplets compared with other cellular components, which suggests that lipid droplets may have a crucial role in cancer therapy. This result is consistent with previous studies suggesting that lipid droplets are potential targets for cancer treatment.[59,60] Lipid droplet alterations can be used as biomarkers for drug response, in that lipid droplet numbers increase in tumor tissues of patients with colorectal adenocarcinoma. Treatment with either aspirin or a fatty acid synthase inhibitor significantly reduces the number of lipid droplets.[59]

The present study indicates that panitumumab treatment of SW48 cells causes changes in the Raman spectra of cellular components, including both intensity changes and wavenumber shifts. These results show for the first time the effect of an EGFR inhibitor on cellular components by label-free Raman spectral imaging. The study also shows that SW480 cells harboring oncogenic K-RAS mutations have essentially no response to panitumumab. This is in agreement with the observed responses of cancer patients with oncogenic K-Ras mutations to anti-EGFR therapies, who fail to respond to panitumumab. We also monitored the effect of panitumumab on SW48 and SW480 cells using the conventional *in vitro* analytical techniques of fluorescence microscopy and Western blotting. Fluorescence labeling of EGFR confirmed that the receptor−panitumumab complex was internalized in SW48 and SW480 cells using the experimental conditions for Raman measurements (Figure S5, SI). The Western blotting analyses of SW48 cells (Figure 6A) indicated that ERK phosphorylation was inhibited by panitumumab compared with that observed in control cells. ERK activity was slightly inhibited by panitumumab in SW480 cells (Figure 6B) but was significantly enhanced by EGF binding. Addition of panitumumab to EGF-treated cells severely inhibited ERK phosphorylation (Figure 6B). Therefore, the Western blot analyses differed from the

DOI: 10.1021/acs.analchem.5b01431
Anal. Chem. 2015, 87, 7297−7304

observed patient responses. We performed several Raman measurements of SW480 cells incubated with either EGF or EGF and panitumumab. The difference spectra of cells treated with EGF versus those treated with EGF and panitumumab revealed no spectral changes (Figures S6 and S7, SI). Thus, Raman spectral images of SW48 and SW480 cells clearly indicate a crucial role for oncogenic K-Ras mutations in the cellular response to panitumumab.

Raman microscopy reflects the overall chemical composition of the cell. This is a crucial difference from conventional assays that measure ERK phosphorylation, or fluorescence microscopy of individual proteins. Signal transduction networks are extremely complex, and silencing of certain pathways can lead to compensation by other pathways.[61−64] Thus, single protein measurements can be misleading. However, the integral changes observed in Raman microscopy directly correlate to biochemical changes induced in cells by a ligand or drug.

The Western blotting results did not significantly discriminate between the K-Ras status in SW48 and SW480 cells. This is perhaps due to effects on ERK phosphorylation caused by cross-talk and compensation among signaling pathways.[1] Our study showed that panitumumab caused significant changes only in SW48 cells but not in SW480 cells (Figure S8, SI). The panitumumab-induced changes observed in SW48 cells can be attributed to the therapeutic effects, which prevent activation of downstream pathways and trigger apoptosis.[65] The Raman results suggest that cell responses to panitumumab are dependent on whether K-Ras is mutated or not. These results are in agreement with several clinical studies, which show the importance of oncogenes such as K-Ras in colorectal cancer therapy as a predictive biomarker for the response to EGFR inhibitors, and a marker for patient selection.[15−17]

CONCLUSIONS

Raman spectral imaging coupled with HCA was used effectively to visualize subcellular components including nuclei, lipid droplets, cytoplasm, and plasma membrane. The effect of ligand binding to EGFR on these components was monitored for the first time by label-free Raman spectral imaging. We examined the effect of the EGFR inhibitor panitumumab on colon cancer cells. The results indicated that the cellular response to panitumumab was dependent on the K-Ras mutation status, which was consistent with the observed responses in patients. The strongest changes in Raman spectra of cancer cells with wild-type K-Ras were observed for lipid droplets. This study opens new approaches for developing an *in vitro*, noninvasive, label-free vibrational spectroscopic test to determine whether a particular drug can be used effectively on patients. The results highlight the power of Raman spectral imaging for probing overall cellular responses compared with the results of conventional techniques such as fluorescence microscopy and Western blotting of single proteins. Our future work will investigate the effects of EGFR inhibitors that target the tyrosine kinase domain and determine the effect of oncogene mutations on the response.

ASSOCIATED CONTENT

Supporting Information

Figures S1−S8 and the method of cytotoxicity assay, Western blot analysis, and fluorescence microscopy. The Supporting Information is available free of charge on the ACS Publications website at DOI: 10.1021/acs.analchem.5b01431.

AUTHOR INFORMATION

Corresponding Author

*Phone: +49-234-32-24461. E-mail: gerwert@bph.rub.

Author Contributions

[§]These authors contributed equally.

Notes

The authors declare no competing financial interest.

ACKNOWLEDGMENTS

We thank Prof. Dr. Axel Mosig and Dr. Erik Freier for useful discussions. This research was supported by the Protein Research Unit Ruhr within Europe (PURE), Ministry of Innovation, Science and Research (MIWF) of North-Rhine Westphalia, Germany; the Center for Vibrational Microscopy (CVM), European Regional Development Fund, European Union and North-Rhine Westphalia, Germany; the Deutsche Forschungsgemeinschaft under grant No. SFB 642.

REFERENCES

(1) Mendoza, M. C.; Er, E. E.; Blenis, J. *Trends Biochem. Sci.* **2011**, *36* (6), 320−328.
(2) Arora, A.; Scholar, E. M. *J. Pharmacol. Exp. Ther.* **2005**, *315* (3), 971−979.
(3) Fischer, B.; Marinov, M.; Arcaro, A. *Cancer Treat. Rev.* **2007**, *33* (4), 391−406.
(4) Pajares, B.; Torres, E.; Trigo, J. M.; Sáez, M. I.; Ribelles, N.; Jiménez, B.; Alba, E. *Clin. Transl. Oncol.* **2012**, *14* (2), 94−101.
(5) Peeters, M.; Price, T.; Van Laethem, J.-L. *Oncologist* **2009**, *14* (1), 29−39.
(6) Capdevila, J.; Elez, E.; Macarulla, T.; Ramos, F. J.; Ruiz-Echarri, M.; Tabernero, J. *Cancer Treatment Rev.* **2009**, *35* (4), 354−363.
(7) Baselga, J. *Eur. J. Cancer* **2001**, *37* (Suppl 4), S16−22.
(8) Mendelsohn, J. *J. Clin. Oncol.* **2003**, *21* (14), 2787−2799.
(9) Brand, T. M.; Iida, M.; Li, C.; Wheeler, D. L. *Discovery Med.* **2011**, *12* (66), 419−432.
(10) Boguski, M. S.; McCormick, F. *Nature* **1993**, *366* (6456), 643−654.
(11) Donovan, S.; Shannon, K. M.; Bollag, G. *Biochim. Biophys. Acta* **2002**, *1602* (1), 23−45.
(12) Downward, J. *Nat. Rev. Cancer* **2003**, *3* (1), 11−22.
(13) Schubbert, S.; Shannon, K.; Bollag, G. *Nature Rev. Cancer* **2007**, *7* (7), 295−308.
(14) Bos, J. L. *Cancer Res.* **1989**, *49* (17), 4682−4689.
(15) Adams, R.; Maughan, T. *Expert Rev. Anticancer Therapy* **2007**, *7* (4), 503−518.
(16) Bardelli, A.; Siena, S. *J. Clin. Oncol.* **2010**, *28* (7), 1254−1261.
(17) Amado, R. G.; Wolf, M.; Peeters, M.; Van Cutsem, E.; Siena, S.; Freeman, D. J.; Juan, T.; Sikorski, R.; Suggs, S.; Radinsky, R.; Patterson, S. D.; Chang, D. D. *J. Clin. Oncol.* **2008**, *26* (10), 1626−1634.
(18) Mavarani, L.; Petersen, D.; El-Mashtoly, S. F.; Mosig, A.; Tannapfel, A.; Kötting, C.; Gerwert, K. *Analyst* **2013**, *138* (14), 4035−4039.
(19) Patel, I. I.; Trevisan, J.; Evans, G.; Llabjani, V.; Martin-Hirsch, P. L.; Stringfellow, H. F.; Martin, F. L. *Analyst* **2011**, *136* (23), 4950.
(20) Popp, J. *Handbook of biophotonics. Vol. 2, Photonics for health care*; Wiley-VC: Weinheim, Germany, 2011.
(21) Matthäus, C.; Chernenko, T.; Newmark, J. A.; Warner, C. M.; Diem, M. *Biophys. J.* **2007**, *93* (2), 668−673.
(22) Krafft, C.; Knetschke, T.; Funk, R. H. W.; Salzer, R. *Anal. Chem.* **2006**, *78* (13), 4424−4429.
(23) Van Manen, H.-J. *Proc. Natl. Acad. Sci. U. S. A.* **2005**, *102* (29), 10159−10164.
(24) Matthäus, C.; Boydston-White, S.; Miljković, M.; Romeo, M.; Diem, M. *Appl. Spectrosc.* **2006**, *60* (1), 1−8.

DOI: 10.1021/acs.analchem.5b01431
Anal. Chem. 2015, 87, 7297−7304

(25) Uzunbajakava, N.; Lenferink, A.; Kraan, Y.; Volokhina, E.; Vrensen, G.; Greve, J.; Otto, C. *Biophys. J.* **2003**, *84* (6), 3968−3981.
(26) Keating, M. E.; Byrne, H. J. *Nanomedicine (Lond)* **2013**, *8* (8), 1335−1351.
(27) Matthäus, C.; Kale, A.; Chernenko, T.; Torchilin, V.; Diem, M. *Mol. Pharmaceutics* **2008**, *5* (2), 287−293.
(28) Chernenko, T.; Sawant, R. R.; Miljkovic, M.; Quintero, L.; Diem, M.; Torchilin, V. *Mol. Pharmaceutics* **2012**, *9* (4), 930−936.
(29) Dorney, J.; Bonnier, F.; Garcia, A.; Casey, A.; Chambers, G.; Byrne, H. J. *Analyst* **2012**, *137* (5), 1111−1119.
(30) Ling, J.; Weitman, S. D.; Miller, M. A.; Moore, R. V.; Bovik, A. C. *Appl. Opt.* **2002**, *41* (28), 6006.
(31) Feofanov, A. V.; Grichine, A. I.; Shitova, L. A.; Karmakova, T. A.; Yakubovskaya, R. I.; Egret-Charlier, M.; Vigny, P. *Biophys. J.* **2000**, *78* (1), 499−512.
(32) Harada, Y.; Dai, P.; Yamaoka, Y.; Ogawa, M.; Tanaka, H.; Nosaka, K.; Akaji, K.; Takamatsu, T. *Histochem. Cell Biol.* **2009**, *132* (1), 39−46.
(33) Salehi, H.; Derely, L.; Vegh, A.-G.; Durand, J.-C.; Gergely, C.; Larroque, C.; Fauroux, M.-A.; Cuisinier, F. J. G. *Appl. Phys. Lett.* **2013**, *102* (11), 113701.
(34) Meister, K.; Niesel, J.; Schatzschneider, U.; Metzler-Nolte, N.; Schmidt, D. A.; Havenith, M. *Angew. Chem., Int. Ed. Engl.* **2010**, *49* (19), 3310−3312.
(35) El-Mashtoly, S. F.; Petersen, D.; Yosef, H. K.; Mosig, A.; Reinacher-Schick, A.; Kötting, C.; Gerwert, K. *Analyst* **2014**, *139* (5), 1155−1161.
(36) Nawaz, H.; Garcia, A.; Meade, A. D.; Lyng, F. M.; Byrne, H. J. *Analyst* **2013**, *138* (20), 6177.
(37) Chan, J.; Fore, S.; Wachsmann-Hogiu, S.; Huser, T. *Laser Photonics Rev.* **2008**, *2* (5), 325−349.
(38) Huser, T.; Orme, C. A.; Hollars, C. W.; Corzett, M. H.; Balhorn, R. *J. Biophotonics* **2009**, *2* (5), 322−332.
(39) Owen, C. A.; Selvakumaran, J.; Notingher, I.; Jell, G.; Hench, L. L.; Stevens, M. M. *J. Cellular Biochem.* **2006**, *99* (1), 178−186.
(40) Nawaz, H.; Bonnier, F.; Knief, P.; Howe, O.; Lyng, F. M.; Meade, A. D.; Byrne, H. J. *Analyst* **2010**, *135* (12), 3070−3076.
(41) Nawaz, H.; Bonnier, F.; Meade, A. D.; Lyng, F. M.; Byrne, H. J. *Analyst* **2011**, *136* (12), 2450−2463.
(42) Matthäus, C.; Chernenko, T.; Newmark, J. A.; Warner, C. M.; Diem, M. *Biophys. J.* **2007**, *93* (2), 668−673.
(43) Scalfi-Happ, C.; Udart, M.; Hauser, C.; Rück, A. *Medical Laser Application* **2011**, *26* (4), 152−157.
(44) Krauß, S. D.; Petersen, D.; Niedieker, D.; Fricke, I.; Freier, E.; El-Mashtoly, S. F.; Gerwert, K.; Mosig, A. *Analyst* **2015**, *140*, 2360−2368.
(45) Krafft, C.; Knetschke, T.; Funk, R. H. W.; Salzer, R. *Anal. Chem.* **2006**, *78* (13), 4424−4429.
(46) Krafft, C.; Neudert, L.; Simat, T.; Salzer, R. *Spectrochim. Acta A Mol. Biomol. Spectrosc.* **2005**, *61* (7), 1529−1535.
(47) Huang, Y.-S.; Karashima, T.; Yamamoto, M.; Hamaguchi, H. *Biochemistry* **2005**, *44* (30), 10009−10019.
(48) Matthäus, C.; Krafft, C.; Dietzek, B.; Brehm, B. R.; Lorkowski, S.; Popp, J. *Anal. Chem.* **2012**, *84* (20), 8549−8556.
(49) El-Mashtoly, S. F.; Niedieker, D.; Petersen, D.; Krauss, S. D.; Freier, E.; Maghnouj, A.; Mosig, A.; Hahn, S.; Kötting, C.; Gerwert, K. *Biophys. J.* **2014**, *106* (9), 1910−1920.
(50) Salzer, R. *Infrared and Raman Spectroscopic Imaging*; Wiley-VCH: Weinheim, 2009.
(51) Diem, M.; Chalmers, J. M.; Griffiths, P. R. *Vibrational Spectroscopy for Medical Diagnosis*; John Wiley & Sons: Hoboken, NJ, 2008.
(52) Murthy, S.; Mathur, S.; Bishop, W. P.; Field, E. J. *J. Lipid Res.* **1997**, *38* (2), 206−216.
(53) Liang, C.-F.; Chao, J. C.-J.; Hwang, S.-M.; Tsai, Y.-H. *IUBMB Life* **2002**, *54*, 275−279.
(54) Vartanian, S.; Bentley, C.; Brauer, M. J.; Li, L.; Shirasawa, S.; Sasazuki, T.; Kim, J.-S.; Haverty, P.; Stawiski, E.; Modrusan, Z.; Waldman, T.; Stokoe, D. *J. Biol. Chem.* **2013**, *288* (4), 2403−2413.
(55) Haigler, H.; Ash, J. F.; Singer, S. J.; Cohen, S. *Proc. Natl. Acad. Sci. U.S.A.* **1978**, *75* (7), 3317−3321.
(56) Nishimura, Y.; Yoshioka, K.; Bereczky, B.; Itoh, K. *Molecular Cancer* **2008**, *7* (1), 42.
(57) Foon, K. A.; Yang, X.-D.; Weiner, L. M.; Belldegrun, A. S.; Figlin, R. A.; Crawford, J.; Rowinsky, E. K.; Dutcher, J. P.; Vogelzang, N. J.; Gollub, J.; Thompson, J. A.; Schwartz, G.; Bukowski, R. M.; Roskos, L. K.; Schwab, G. M. *Int. J. Radiat. Oncol. Biol. Phys.* **2004**, *58* (3), 984−990.
(58) You, B.; Chen, E. X. *J. Clin. Pharmacol.* **2012**, *52* (2), 128−155.
(59) Accioly, M. T.; Pacheco, P.; Maya-Monteiro, C. M.; Carrossini, N.; Robbs, B. K.; Oliveira, S. S.; Kaufmann, C.; Morgado-Diaz, J. A.; Bozza, P. T.; Viola, J. P. B. *Cancer Res.* **2008**, *68* (6), 1732−1740.
(60) Tirinato, L.; Liberale, C.; Di Franco, S.; Candeloro, P.; Benfante, A.; La Rocca, R.; Potze, L.; Marotta, R.; Ruffilli, R.; Rajamanickam, V. P.; Malerba, M.; De Angelis, F.; Falqui, A.; Carbone, E.; Todaro, M.; Medema, J. P.; Stassi, G.; Di Fabrizio, E. *Stem Cells* **2015**, *33*, 35−44.
(61) Pimienta, G.; Pascual, J. *Cell Cycle* **2007**, *6* (21), 2628−2632.
(62) Futran, A. S.; Link, A. J.; Seger, R.; Shvartsman, S. Y. *Curr. Biol.* **2013**, *23* (21), R972−979.
(63) Poulikakos, P. I.; Zhang, C.; Bollag, G.; Shokat, K. M.; Rosen, N. *Nature* **2010**, *464* (7287), 427−430.
(64) Burns, M. C.; Sun, Q.; Daniels, R. N.; Camper, D.; Kennedy, J. P.; Phan, J.; Olejniczak, E. T.; Lee, T.; Waterson, A. G.; Rossanese, O. W.; Fesik, S. W. *Proc. Natl. Acad. Sci. U. S. A.* **2014**, *111* (9), 3401−3406.
(65) Pfeiffer, P.; Qvortrup, C.; Eriksen, J. G. *Oncogene* **2007**, *26* (25), 3661−3678.

DOI: 10.1021/acs.analchem.5b01431
Anal. Chem. 2015, 87, 7297−7304